Please cite as: Finnegan, W.; Fagan, E.; Flanagan, T.; Doyle, A.; Goggins, J. (2020) Operational fatigue loading on tidal turbine blades using computational fluid dynamics. Renewable Energy, 152, p430-440DOI: 10.1016/j.renene.2019.12.154.

Operational fatigue loading on tidal turbine blades using computational fluid dynamics

William Finnegan [a,b,c,*], Edward Fagan [a,b], Tomas Flanagan [c], Adrian Doyle [c], Jamie Goggins [a,b,**]

[a] *Civil Engineering, School of Engineering, National University of Ireland Galway, Galway, Ireland*
[b] *MaREI Centre, Ryan Institute, National University of Ireland Galway, Galway, Ireland*
[c] *ÉireComposites Teo, An Choill Rua, Inverin, Co. Galway, Ireland*

Corresponding authors' email addresses: * william.finnegan@nuigalway.ie (W. Finnegan)
** jamie.goggins@nuigalway.ie (J. Goggins)

Abstract

As the world moves to a greater reliance on renewable energy, a vital component will be the predictability and dependability of the energy source; tidal energy provides such a solution. Horizontal axis tidal turbines are the most mature technology of all the marine renewable energy devices currently under development, as full-scale porotypes are already being tested and operated. As the industry develops and strives for commercial viability, it is becoming increasingly vital to develop a robust understanding of the complex interaction between the tidal flow, turbine blades and the support structure. This study uses an advanced computational fluid dynamics model to explore the operational fatigue loadings induced on tidal turbine blades. Two factors are considered, the presence of a support structure and varying vertical velocity profile of the tidal current. In order to perform the investigation, a model of a concept 16m diameter horizontal axis tidal turbine with a monopile support structure is created. An investigation of the operational fatigue loadings due to variations in the positioning and the diameter of the support structure, the tidal turbine blade loads were found to varying by up to 43% of the maximum total thrust force.

Keywords: Computational fluid dynamics; Fatigue loading; Fluid-structure interaction; Tidal energy; Tidal turbine; Unsteady loading.

Abbreviations

ADCP	Acoustic Doppler current profiler
BEMT	Blade element momentum theory
CAPEX	Capital expenditure
CFD	Computational fluid dynamics
EMEC	European Marine Energy Centre
EU	European Union
GGI	General Grid Interface
HATT	Horizontal axis tidal turbine
OPEX	Operational expenditure
RANSE	Reynolds-averaged Navier Stokes equations
SST	Shear stress transport
TRL	Technology readiness level
TSR	Tip speed ratio

Please cite as: Finnegan, W.; Fagan, E.; Flanagan, T.; Doyle, A.; Goggins, J. (2020) Operational fatigue loading on tidal turbine blades using computational fluid dynamics. Renewable Energy, 152, p430-440DOI: 10.1016/j.renene.2019.12.154.

1 Introduction

In recent years, there has been a growing interest in establishing renewable sources of marine energy to alleviate the global reliance on fossil fuels. The Ocean Energy Strategic Roadmap for the European Union (EU) predicts that with favourable support to the nascent industry in the coming decades, the global market in marine renewable energy could be worth €653bn between 2010 and 2050 [1]. Tidal energy, with its reliability and predictability, is developing into the ocean energy sector with the greatest potential. Recently, there has been a number of examples of its commercial maturity, including Orbital Marine Power's O2-2000 tidal current turbine generating 1.2 GWh of electricity over a 5 month period in 2017 [2] and the MeyGen project, which will deliver the installation of four 1.5MW turbines offshore in an array as well as the construction of the onshore infrastructure [1]. It is envisaged, based on projects that have been awarded public funds, that 71 MW of tidal stream energy capacity could be operational within the EU in 2020 and this could potentially reach 600 MW if technological and financial barriers are overcome [3]. Currently, the EU is at the forefront of technology development as approximately 50 % of tidal energy developers are located within the EU, along with the majority of ocean energy infrastructure [3]. Additionally, based on a EU report by Corsatea and Magagna [4], 76 % of research and development efforts in the tidal energy sector are related to horizontal axis tidal turbine (HATT) technologies.

In order for tidal energy technologies to develop at an efficient and effective rate, computational modelling is vital. It provides an efficient approach to innovate device designs as devices move through the technology readiness levels (TRLs), improving specific components of the devices as the objectives change from energy capture to structural response and reducing the levelised cost of energy. Currently within the tidal energy sector, the most commonly used computational modelling method for estimating the hydrodynamic loads on HATT is based on the blade element momentum theory (BEMT) [5]. However, as traditional BEMT codes do not take account of three-dimensional flow effects, it is necessary to make a number of modifications (or corrections) to the code to improve the model's accuracy for a wider range of operating conditions, which is demonstrated by Masters et al. [6]. The ability of BEMT to predict the loadings and performance of model-scale tidal turbines has been demonstrated by Bahaj et al. [7] for uniform inflow conditions, O'Rourke et al. [8] for non-uniform inflow conditions, Galloway et al. [9] for wave-current interactions and Fagan [10] for uniform flow conditions and for inflow conditions based on real world data.

However, as computational capabilities grow, computational fluid dynamics (CFD) has gained popularity as it presents a more accurate and versatile analysis tool, when compared to traditional BEMT. Its popularity is evident in the number of recent publications applying the CFD Reynolds-averaged Navier Stokes equations (RANSE) models to investigate HATT performance, which are summarised in Table 1. Based on the selection of studies detailed in Table 1, the most commonly used commercial software has been ANSYS CFX and the most commonly employed turbulence model is the shear stress transport (SST) model. The effect of including a support structure connected to the tidal turbine hub, which would be the case in operation, has been explored in a number of studies. For example, Badshah et al. [11] developed a numerical fluid-structure interaction model, which coupled a CFD model with finite element analysis, and investigated loading variations and fatigue life of a full-scale tidal turbine under the effect of velocity profile, where the variation in flap-wise bending moment coefficient increased from 4.9% to 19%. Additionally, Frost et al. [12] used a CFD model to investigate the performance of Cardiff University's concept tidal turbine with the support structure located either upstream or downstream. They also investigated the effect of varying the proximity between the rotating plane of the turbine and its support stanchion for a constant flow velocity of 3.086 m/s (6 knots). Frost et al. [12] presents details of the thrust force and bending moment on the

Please cite as: Finnegan, W.; Fagan, E.; Flanagan, T.; Doyle, A.; Goggins, J. (2020) Operational fatigue loading on tidal turbine blades using computational fluid dynamics. Renewable Energy, 152, p430-440DOI: 10.1016/j.renene.2019.12.154.

tidal turbine blade as it rotates through 360°, demonstrating significant fluctuations as the blade passes the support stanchion. Ahmed et al. [13] explored the fluctuating loads on a 1MW tidal turbine at the European Marine Energy Centre (EMEC) test site in Scotland due to velocity shear and turbulence. The analysis was initially performed using a CFD model based on RANSE, followed by a large eddy simulation model, which was compared and validated against physical test data. Similarly to Frost et al., Ahmed et al. [13] presented results for the fluctuation in thrust force, power coefficient and bending moment on the tidal turbine blade as it rotates through 360°. Furthermore, significant fluctuations in thrust force and torque have been observed by Jeffcoate et al. [14] during full-scale trials of a 50kW tidal turbine. There are four main aspects that that have been identified by tidal turbine developers that contribute to unsteady loadings on tidal turbine blades:

- Variation in vertical velocity profile of the tidal flow [15];
- Shadow effects from the support structure [16, 17];
- Forces generated from surface waves [18, 19]; and
- Turbulence in incoming tidal flow [20].

Table 1: Summary of previously published studies exploring the use of CFD to examine the operation of horizontal axis tidal turbines

Reference	Numerical method	Commercial code	Turbulence model	Support structure	Wave included	Wake analysed
Badshah et al. [11]	RANSE	ANSYS CFX	SST	Yes	No	Yes
Badshah et al. [28]	RANSE	ANSYS CFX	SST	No	No	No
Aparna et al. [29]	RANSE	ANSYS Fluent	SST	No	No	No
Tatum et al. [30]	RANSE	ANSYS CFX	SST	Yes	Yes	No
Gebreslassie et al. [31]	RANSE + IBF	OpenFOAM	k-ω SST	No	Yes	Yes
Kulkarni et al. [32]	RANSE	ANSYS CFX	k–ε model & SST	No	No	No
Frost et al. [12]	RANSE	ANSYS CFX	SST	Yes	No	No
Holst et al. [33]	RANSE	ANSYS CFX	SST	No	Yes	Yes
Noruzi et al. [34]	RANSE	ANSYS CFX	SST	No	No	No
Wang and Day [35]	RANSE	FLUENT	k-ω SST	No	Yes	No
Jo et al. [36]	RANSE	ANSYS CFX	SST	Yes	No	No
Kang et al. [37]	CURVIB	N/A	N/A	Yes	No	Yes
Turnock et al. [38]	Coupled RANSE-BEMT	ANSYS CFX	k–ε model	No	No	Yes
Faudot and Dahlhaug [39]	RANSE	ANSYS CFX	SST	No	Yes	No
O'Doherty et al. [40]	RANSE	FLUENT	RSM	No	No	No

Legend: Curvilinear immersed boundary method (CURVIB); Not applicable (N/A); Reynolds-averaged Naiver Stokes equations (RANSE); Reynolds Stress model (RSM); Shear Stress Transport (SST).

In this paper, a numerical CFD model is developed to investigate the contribution of the first two of these effects (variation in vertical velocity profile of the tidal flow; and shadow effects from the support structure) to the operational fatigue loading on the tidal turbine blades. It is important to note that the support structure causes a shadow effect regardless if it is upstream or in the wake of the turbine, which is evident in the results of Frost et al. [12]. For the purpose of this study, a vertical support structure with a circular cross-section is specified, which supports the turbine hub and is anchored at the sea floor. The circular cross-section (similar to a monopile structure) is assumed for

Please cite as: Finnegan, W.; Fagan, E.; Flanagan, T.; Doyle, A.; Goggins, J. (2020) Operational fatigue loading on tidal turbine blades using computational fluid dynamics. Renewable Energy, 152, p430-440DOI: 10.1016/j.renene.2019.12.154.

ease of manufacture, which is the same assumption used by Frost et al. [12], and support structures of various diameters are also investigated. The support structure is positioned immediately in either the front or the wake of the turbine in order to quantify its effect during the flood and ebb tides (assuming the turbine cannot yaw into the oncoming flow). The tidal current flow profile has been derived from acoustic Doppler current profiler (ADCP) data, which was recorded at a site off the Scottish coast. The results of this study will provide designers, manufacturers and developers of tidal energy devices with insights into the suitable design criteria for fatigue loading over the operational lifespan of blades.

2 Materials and methods

2.1 Turbine geometry

For the purpose of this study, a concept 16 m diameter HATT was employed, designed using the methodology detailed in [10]. The blade hydrodynamic shape is generated using the NACA63xxx series of blade profiles and the distribution of the chord length, hydrodynamic twist angle and the section shapes along the length of the turbine blade are summarised in Table 2. A schematic detailing the numerical calculation domains, which includes the rendered turbine blades, hub and support structure, is shown in Figure 1. It is assumed that the height of the hub of the turbine, z_{hub}, is located at 16.5 m (z_{hub}/R = 2.02) above the sea floor, where the total water depth, d, is 40 m (d/R = 4.91). The support structure, which is similar to a monopile structure, extends from the turbine hub to the sea floor and is located immediately in either the front or the wake of the turbine.

Table 2: Geometry of the tidal turbine used in the analysis

Radius (m)	*Chord (m)*	*Twist (°)*	*Section*
0.5	0.50	0.0	Circular
1.0	1.45	18.0	NACA 63-225
1.5	1.40	15.5	NACA 63-222
2.0	1.30	13.5	NACA 63-220
2.5	1.20	11.5	NACA 63-218
3.0	1.05	10.0	NACA 63-216
3.5	0.95	9.0	NACA 63-215
4.0	0.85	8.0	NACA 63-214
4.5	0.80	7.0	NACA 63-213.5
5.0	0.775	6.0	NACA 63-213
5.5	0.725	5.0	NACA 63-212.5
6.0	0.70	4.0	NACA 63-212
6.5	0.65	3.5	NACA 63-212
7.0	0.60	3.0	NACA 63-212
7.5	0.575	2.5	NACA 63-212
8.0	0.55	2.5	NACA 63-212
8.15	0.25	2.5	NACA 63-212

2.2 CFD model details

The CFD model used in this study has been developed using the commercial software package ANSYS CFX (version 17.1) [21], which uses a finite volume method to solve the RANSE. ANSYS CFX is fully integrated with ANSYS Workbench and, therefore, can be easily coupled with other ANSYS simulation technologies.

Please cite as: Finnegan, W.; Fagan, E.; Flanagan, T.; Doyle, A.; Goggins, J. (2020) Operational fatigue loading on tidal turbine blades using computational fluid dynamics. Renewable Energy, 152, p430-440DOI: 10.1016/j.renene.2019.12.154.

2.2.1 The Governing Equations

The method that the ANSYS CFX solver is based on is the finite volume technique [18]. This technique divides the region of interest into sub-regions and discretises the governing equations in order to solve them iteratively over each sub-region. Therefore, an approximation of the value of each variable at points throughout the domain is achieved.

The governing equations solved by the ANSYS CFX solver include the mass continuity equation, which is given as:

$$\frac{\partial \rho}{\partial t} + \frac{\partial(\rho u_1)}{\partial x} + \frac{\partial(\rho u_2)}{\partial y} + \frac{\partial(\rho u_3)}{\partial z} = 0 \tag{1}$$

and the 3-dimensional Navier-Stokes equations, which are given as:

$$\rho\left(\frac{\partial u_1}{\partial t} + u_1\frac{\partial u_1}{\partial x} + u_2\frac{\partial u_1}{\partial y} + u_3\frac{\partial u_1}{\partial z}\right) = -\frac{\partial p}{\partial x} + 2\mu\frac{\partial^2 u_1}{\partial x^2} + \frac{\partial}{\partial y}\left(\mu\left(\frac{\partial u_1}{\partial y} + \frac{\partial u_2}{\partial x}\right)\right) + \frac{\partial}{\partial z}\left(\mu\left(\frac{\partial u_1}{\partial z} + \frac{\partial u_3}{\partial x}\right)\right) + F_1 \tag{2}$$

$$\rho\left(\frac{\partial u_2}{\partial t} + u_1\frac{\partial u_2}{\partial x} + u_2\frac{\partial u_2}{\partial y} + u_3\frac{\partial u_2}{\partial z}\right) = -\frac{\partial p}{\partial y} + 2\mu\frac{\partial^2 u_2}{\partial y^2} + \frac{\partial}{\partial x}\left(\mu\left(\frac{\partial u_1}{\partial y} + \frac{\partial u_2}{\partial x}\right)\right) + \frac{\partial}{\partial z}\left(\mu\left(\frac{\partial u_2}{\partial z} + \frac{\partial u_3}{\partial y}\right)\right) + F_2 - \rho g \tag{3}$$

$$\rho\left(\frac{\partial u_3}{\partial t} + u_1\frac{\partial u_3}{\partial x} + u_2\frac{\partial u_3}{\partial y} + u_3\frac{\partial u_3}{\partial z}\right) = -\frac{\partial p}{\partial z} + 2\mu\frac{\partial^2 u_3}{\partial z^2} + \frac{\partial}{\partial x}\left(\mu\left(\frac{\partial u_1}{\partial z} + \frac{\partial u_3}{\partial x}\right)\right) + \frac{\partial}{\partial y}\left(\mu\left(\frac{\partial u_3}{\partial y} + \frac{\partial u_2}{\partial z}\right)\right) + F_3 \tag{4}$$

where t is time, ρ is the fluid density, x, y, z are Cartesian coordinates (as shown in Figure 1), u_1 is the flow velocity in the x-direction, u_2 is the flow velocity in the y-direction, u_3 is the flow velocity in the z-direction, F_1 is the body force on the fluid in the x-direction, $F_2 - \rho g$ is the body force on the fluid in the y-direction (vertical), F_3 is the body force on the fluid in the z-direction, p is pressure and μ is viscosity.

2.2.2 CFD model set-up and solver stage

The CFD model used for this study has been developed based on a similar method to that described in detail in Finnegan et al. [22]. The set-up for the CFD model is divided into three stages: (i) the

Please cite as: Finnegan, W.; Fagan, E.; Flanagan, T.; Doyle, A.; Goggins, J. (2020) Operational fatigue loading on tidal turbine blades using computational fluid dynamics. Renewable Energy, 152, p430-440DOI: 10.1016/j.renene.2019.12.154.

geometry, (ii) the computational domain and mesh and (iii) the solver physics, which includes the analysis type and the boundary conditions.

The geometry of the turbine, which has been defined in the previous section, is defined in the CFD model and enclosed in a rotating fluid region. This domain is itself enclosed in a larger stationary fluid domain, as can be seen in Figure 1. A region size dependency study was conducted to determine an efficient size for the computational domain. Both the rotating and stationary domains are cylindrical in shape.The rotating domain is 17 m in diameter (2.09R) with a thickness of 2 m (0.25R) and the stationary domain is 40 m in diameter (4.91R) with a total length of 110 m (13.5R). The support structure for the turbine hub is located in the outer stationary domain, immediately in either the front or the wake of the turbine, as shown in Figure 1.

Based on the study detailed in Finnegan et al. [22], the primary mesh refinement is required within the rotating domain and at the turbine wall. This approach allows for efficient modelling times, where the overall size of the mesh is minimised, reducing the computational requirements. Therefore, a maximum element size of 0.1 m was specified on the turbine wall boundaries (using the “face sizing” mesh refinement option in ANSYS CFX) and a maximum element size of 0.175 m was specified within the rotating domain. Within the stationary domain, the maximum element size was specified as 1.2 m as further mesh refinement did not improve the accuracy of the model. Overall, the total mesh size is approximately 370,000 nodes (or approximately 2 million elements). A schematic of the mesh, which shows the refinement around the turbine wall and support structure, can be seen in Figure 2.

Similarly to the studies summarised in Table 1, the turbulence model used in this analysis is the SST. Since a transient simulation is necessary, the "transient rotor-stator" method, also known as the “sliding mesh approach”, is specified within the rotating domain.The stationary flow is solved in a fixed frame of reference and the rotating flow field is solved in a rotating frame of reference, where the Coriolis force is included as part of the source terms. A general connection between the stationary and rotating fluid domains is specified. The rotational speed of the region is defined, along with a General Grid Interface (GGI) mesh connection. An inflow boundary condition is specified at one end of the stationary domain and an ‘opening’ boundary condition, with a pressure specified at 0 Pa, at the other end. The outer curved edge of the stationary domain is defined as a wall boundary with a free slip condition. A velocity profile is applied at the inflow boundary, which is specified at either:

- A constant velocity of 2.25m/s, or
- The mean tidal flow, based on ADCP site data for the Pentland Firth (detailed in Section 2.3).

Once the model has been set-up, a ‘solver’ stage takes place in order to calculate the final solution. Within the solver, the transient scheme is a Second Order Backward Euler scheme and the convergence criteria is set to $1e^{-4}$ of the root mean square residual.

2.3 Mean tidal flow

The mean tidal flow used in this study has been derived from ADCP data for the Inner Sound, Pentland Firth in Scotland. The data consists of ADCP measurements of depth-wise tidal current magnitudes and directions for approximately a month period from February to March 2013 [23]. The ADCP device used was a Telydyne Workhorse Sentinel and the instrument was deployed at a depth of approximately 34 m, where the water depth varied between 32.6 m and 36 m over the recorded month. The mean tidal flow profile used in this study, which is derived from this ADCP data, is shown graphically in Figure 3 (b). Additional details on the processing of the raw ADCP data can be found in Fagan [10].

Please cite as: Finnegan, W.; Fagan, E.; Flanagan, T.; Doyle, A.; Goggins, J. (2020) Operational fatigue loading on tidal turbine blades using computational fluid dynamics. Renewable Energy, 152, p430-440DOI: 10.1016/j.renene.2019.12.154.

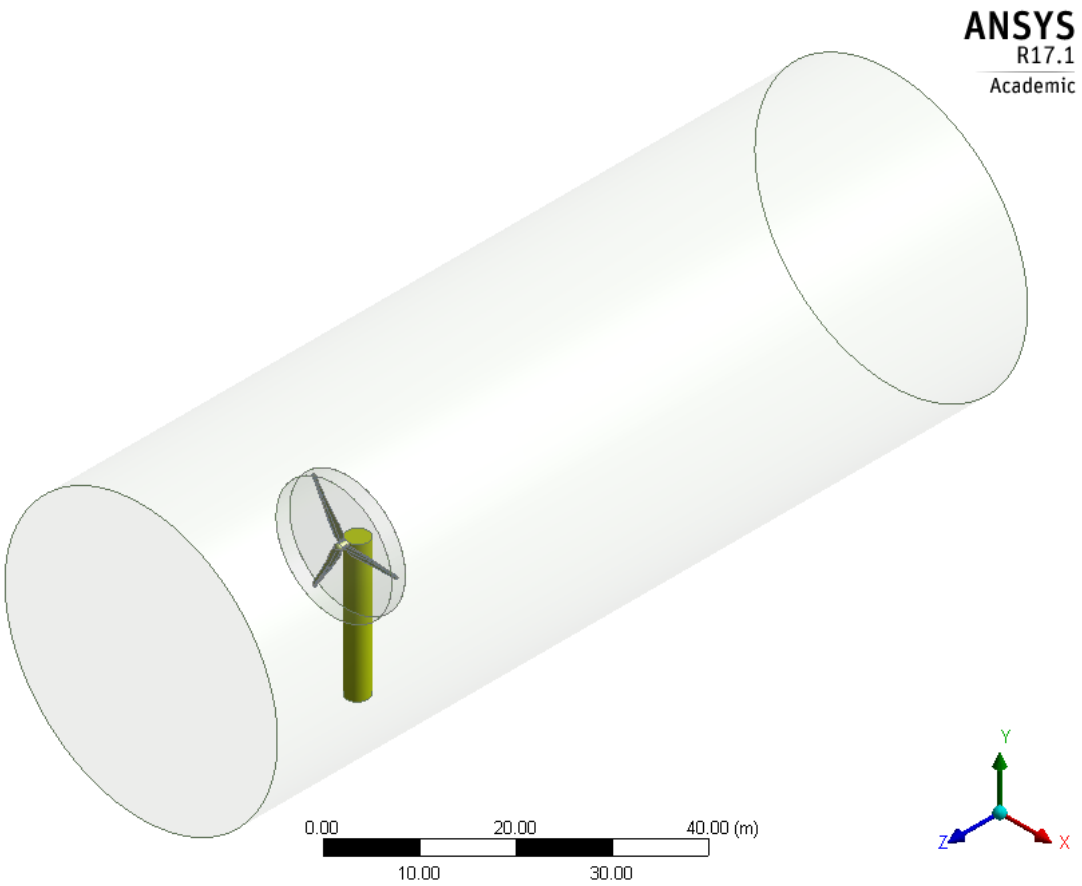

Figure 1: Schematic of the model geometry for the analysis, where the turbine and support structure are rendered.

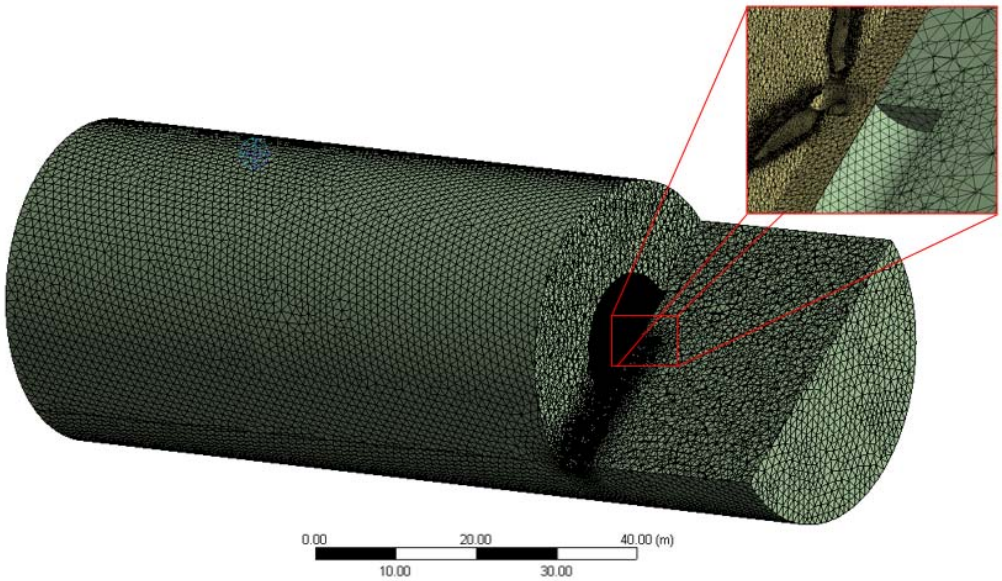

Figure 2: Illustration of the mesh used in the simulation that includes the necessary mesh refinement, where the support structure is placed in front of the turbine

Please cite as: Finnegan, W.; Fagan, E.; Flanagan, T.; Doyle, A.; Goggins, J. (2020) Operational fatigue loading on tidal turbine blades using computational fluid dynamics. Renewable Energy, 152, p430-440DOI: 10.1016/j.renene.2019.12.154.

2.4 CFD model comparison

The accuracy of the CFD model is assessed by comparing the results of steady state simulations of a tidal turbine (with no support structure present) for a number of tip speed ratios (TSRs), ranging from 2 to 8, to results from a BEMT model analysis of the same tidal turbine [10]. In both analyses, the same constant inflow velocity of 2.5 m/s is specified. As no support structure is present and the flow velocity is constant, it is assumed that there is a quasi-steady flow around the rotating tidal turbine at every rotation angle and, therefore, a steady state CFD simulation can be performed. In order to take account of the rotation of the tidal turbine, additional rotational effects (Coriolis and centrifugal terms) are imparted to the flow as source terms in the RANSE in the rotating domain, which is achieved by specifying a "frozen rotor" method for the rotating domain within the ANSYS CFX model. In order to compare the results of the two analyses, the same non-dimensionalised coefficients (*TSR*, power (C_P) and thrust (C_T) coefficients) are used in both models, which are defined using the following equations [5]:

$$TSR = \frac{\Omega R}{U_T} \tag{5}$$

$$C_P = \frac{Q\Omega}{\frac{1}{2}\rho U_T^3 A} \tag{6}$$

$$C_T = \frac{T}{\frac{1}{2}\rho U_T^2 A} \tag{7}$$

where Ω is the rotational speed of the turbine (rad/s), R is the radius of the turbine (m), U_T is the average tangential flow velocity (m/s), Q is the rotor torque (Nm), T is the thrust force (N) and A is the area of the turbine (m^2).

Figure 4 compares the results of the two analyses for TSRs from 2 to 8. The CFD model under predicts the power coefficient, C_P, of the turbine at the lower TSRs, where the C_P in the CFD model is 52-70% of that predicted by the BEMT model. However, the C_P produced from the CFD model agrees closely with the BEMT model from approximately TSR = 5 and high TSRs, where the difference is reduced to less than 11%. For the thrust coefficient, C_T, the CFD model predictions are in close agreement with the BEMT model for the lower TSRs. However, the CFD model somewhat over predicts the C_T, compared to the BEMT model, by 10-13% at higher TSRs. Overall, the comparison presented in Figure 4 suggests reasonable agreement between the solutions. The differences in the two models are due to (i) the CFD model including nonlinear viscous effects around the hub and turbine blades, particularly at the tip, (ii) the effect of flow moving parallel to the blade length and (iii) minor effects due to the interaction between the rotating turbine and the outer curved wall boundary. Although losses due to the hub and tip effects have been included in the BEMT model, many of the other effects are not included. From a computational point-of-view, the BEMT model is significantly less computationally expensive and, therefore, is a much more useful method for the preliminary design and analysis of turbine blades. However, as the problem increases in complexity (similar to the introduction of a support structure that is detailed in this paper), the CFD approach may prove a much more reliable analysis tool.

2.5 Analysis methodology

Once the CFD model was set up and its accuracy was assessed using a steady state analysis, a number of transient analyses were performed under varying conditions. A summary of the analysis

Please cite as: Finnegan, W.; Fagan, E.; Flanagan, T.; Doyle, A.; Goggins, J. (2020) Operational fatigue loading on tidal turbine blades using computational fluid dynamics. Renewable Energy, 152, p430-440DOI: 10.1016/j.renene.2019.12.154.

configurations used in this study is given in Table 3. Firstly, in order to assess the effect of the variation in vertical velocity profile of the tidal flow, a constant flow condition of 2.25 m/s was specified in one model and a mean tidal flow condition (based on ADCP data recorded at Pentland Firth in Scotland that is described in Section 2.3 and is given in Figure 3) is specified in another. For both models, a constant rotational velocity of 15 rpm has been specified. In order to explore the shadow effects from the support structure for each these flow conditions, a structure (supporting the turbine hub and anchored at the sea floor) is introduced into the model either in front or in the wake of the turbine. In this analysis, the support structure, which has a circular cross section, is positioned in the stationary domain, where the distance between the closest point on the support structure and the centreline of the tidal turbine, x_{ss}, is 1.25 m ($x_{ss}/R = 0.15$) when it is in front of the turbine and 0.75 m ($x_{ss}/R = 0.09$) when it is in the wake of the turbine. Three diameters for the support structure, d_{ss}, are investigated in the study, which are 1 m, 2 m and 3 m (Table 3). The thrust force and torque on the blades, hub and support structure are then compared to the baseline analysis (where no support structure was specified) in order to determine the magnitude of the effect of the support structure.

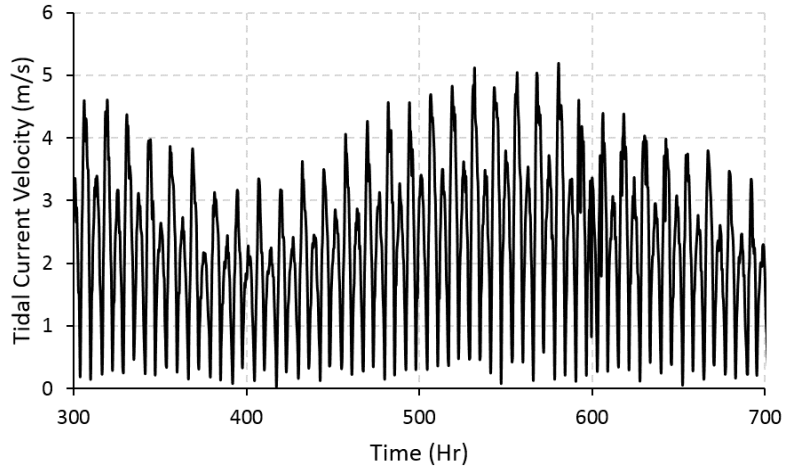

(a)

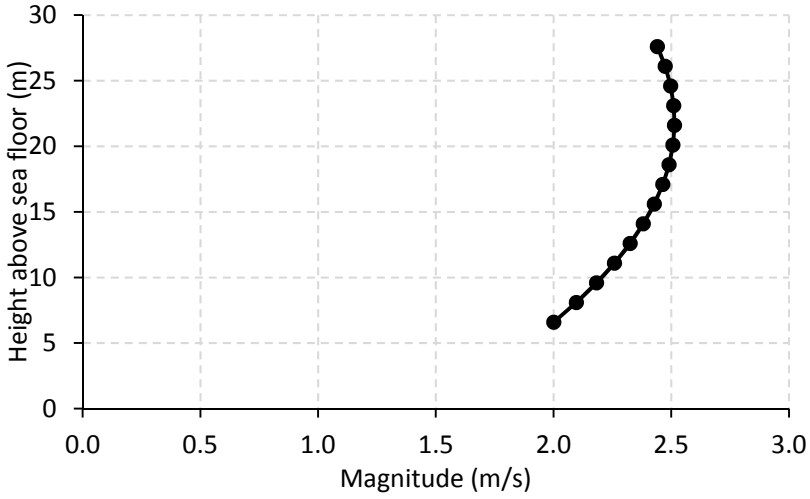

(b)

Figure 3: ADCP measurements obtained at the Pentland Firth site, where (a) is a sample of the tidal velocity data at the depth of the turbine hub (16.5m above the sea floor) and (b) is a profile of the mean tidal velocity, which is used in this study

Please cite as: Finnegan, W.; Fagan, E.; Flanagan, T.; Doyle, A.; Goggins, J. (2020) Operational fatigue loading on tidal turbine blades using computational fluid dynamics. Renewable Energy, 152, p430-440DOI: 10.1016/j.renene.2019.12.154.

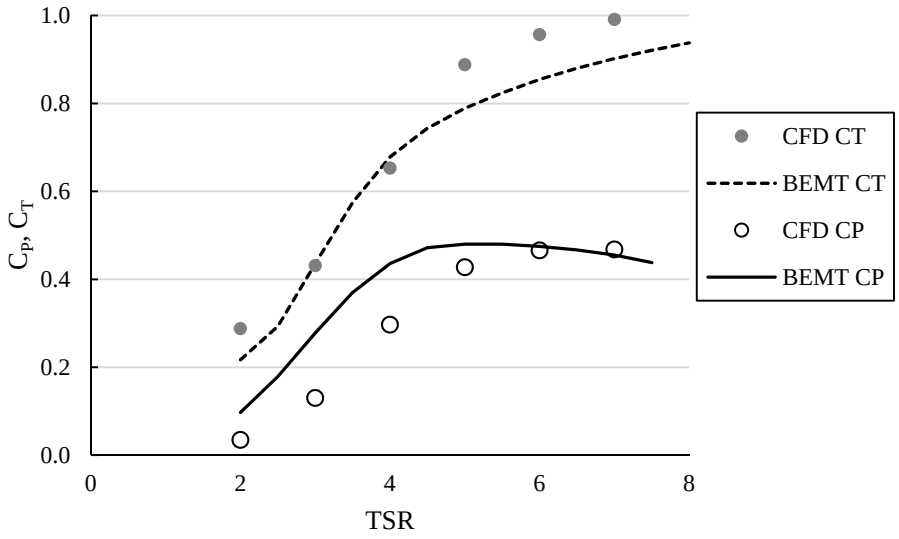

Figure 4: Comparison between the CFD and BEMT [10] predictions for the power and thrust coefficients of the turbine (C_P and C_T, respectively).

Table 3: Summary of the analysis configurations used in this study, where d_{ss} is the diameter of the support structure

Analysis No.	Flow regime	Support structure		
		Diameter, d_{ss} (m)	In turbine wake	In front of turbine
1	2.25 m/s	N/A	N/A	N/A
2	2.25 m/s	1	✓	
3	2.25 m/s	2	✓	
4	2.25 m/s	3	✓	
5	2.25 m/s	1		✓
6	2.25 m/s	2		✓
7	2.25 m/s	3		✓
8	Mean Flow[1]	N/A	N/A	N/A
9	Mean Flow[1]	1	✓	
10	Mean Flow[1]	2	✓	
11	Mean Flow[1]	3	✓	
12	Mean Flow[1]	1		✓
13	Mean Flow[1]	2		✓
14	Mean Flow[1]	3		✓

Legend: [1] Mean tidal flow based on ADCP data recorded at Pentland Firth in Scotland, which is described in Section 2.3 and illustrated graphically in Figure 3 (b); Not applicable (N/A).

3 Results and discussion

For each of the analysis cases, which are described in Section 2.5 and summarised in Table 3, the following variables were monitored:

- Total thrust force on the three blades
- Thrust force on each blade
- The forces on the hub and the support structure
- Total torque on the three blades
- Torque on each individual blade

Please cite as: Finnegan, W.; Fagan, E.; Flanagan, T.; Doyle, A.; Goggins, J. (2020) Operational fatigue loading on tidal turbine blades using computational fluid dynamics. Renewable Energy, 152, p430-440DOI: 10.1016/j.renene.2019.12.154.

An example of the monitored variables is presented in Figure 5 for a 3 m support structure placed in the wake of the turbine with a mean tidal flow specified. It is evident from Figure 5 (a) that the magnitude of the variation in the thrust force on the individual blades is quite significant, but the variation is reduced when the total thrust force on all of the blades is assessed. Additionally, it can be seen in Figure 5 (b) that there is an even more significant variation in the magnitude of torque on the blades and, again, this variation is reduced when the total torque on all of the blades is assessed.

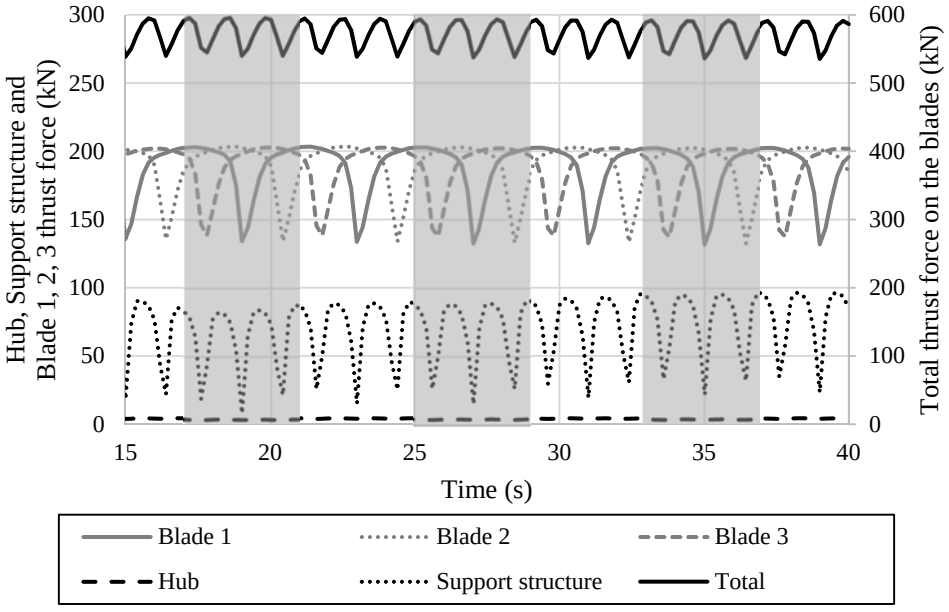

(a)

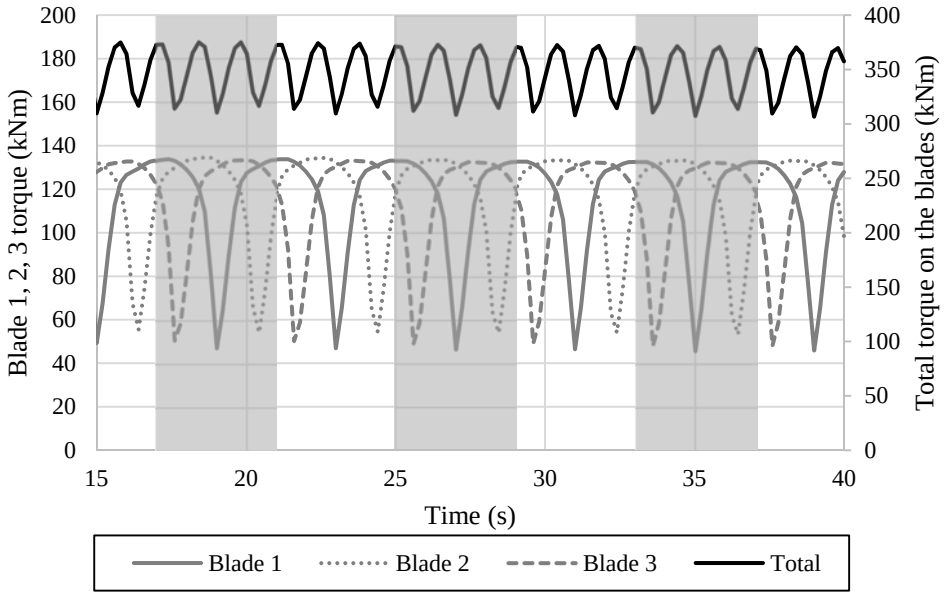

(b)

Figure 5: Variation over time of (a) thrust force (kN) and (b) torque (kNm) on the blades, hub, support structure with a diameter of 3m, which is placed in the wake of the turbine, due to the mean tidal flow at Pentland Firth in Scotland (described in Section 2.3). The grey regions help to signify when Blade 1 rotates from the vertically upward position around 360^{o}.

Please cite as: Finnegan, W.; Fagan, E.; Flanagan, T.; Doyle, A.; Goggins, J. (2020) Operational fatigue loading on tidal turbine blades using computational fluid dynamics. Renewable Energy, 152, p430-440DOI: 10.1016/j.renene.2019.12.154.

The force on the support structure and the hub are included in Figure 5 (a). The thrust force on the hub is relatively small compared to the other components being analysed and this is as a result of its relatively small surface area. However, it is evident from this figure that the thrust force on the support structure is significant, with its variation in magnitude being comparable to that observed for each of the blades, which is due to the shadowing of the tidal flow by the three blades on each rotation. This information would be vital for the structural design of the support structure and for the structural and geotechnical design of the foundations. However, for the purpose of this study, the variations of thrust force and torque on the tidal turbine blades are the main focus.

In the present study, the blades rotate in a clockwise direction and this has an effect on the distribution of the shadow effect on the support structure. In order to describe the motion of the tidal turbine blades, a coordinate system has been adopted, where 0^o indicates the blade is oriented vertically upwards and then rotates 360^o clockwise. The influence of the support structure on the thrust force on the blade is significant and this is evident from the results presented in Figure 6 and Figure 8. As the blade rotates, the thrust force on the blade begins to reduce at approximately 150^o until it reaches 240^o, where the support structure has maximum impact. The blade is oriented vertically downwards at 180^o. Therefore, the effect on the thrust force on each blade lasts twice the angular rotation (60°) passed the centreline of the support structure at 180^o, compared to before reaching it (30°). Overall, it can be seen that the reduction in thrust force on the blade is greater when the support structure is placed in front of the tidal turbine, rather than in its wake. Furthermore, as the diameter of the support structure is increased, the reduction in thrust force on the blade increases (Figure 6 and Figure 8).

Interestingly, for the torque on the turbine blades, as the blade rotate, there is a decrease in torque between approximately 130^o and 230^o (Figures 7 and 9). This is followed by an immediate increase in torque between approximately 230^o and 310^o. However, it is also evident that this increase in torque on the blade, during this part of the rotation, is more significant when the support structure is placed in front of the turbine, rather than in the wake of the turbine. This effect is, in part, caused by the increase in flow velocity as the flow moves around the support structure. However, the total torque is reduced with the presence of the support structure either in front or in the wake of the turbine. Additionally, the magnitude of the reduction in torque on the blade is similar to that observed with the thrust force on the blade, where it is greater with a larger diameter of the support structure or if it is placed in front of the tidal turbine, rather in the wake of the tidal turbine.

In order to analyse the results of the study, the percentage difference between the maximum and minimum total thrust force and total torque as the blade rotates around 360^o has been calculated. For the baseline case with a mean tidal flow condition specified, a 9% difference in the thrust force on each blade was observed. Additionally, as expected, the difference in the total thrust force on the blade when there was a constant flow condition specified was insignificant (less than 1%).The difference in torque on a blade as it rotates around 360^o is just over 1% and 18% for the constant flow and mean flow conditions, respectively. However, a more significant difference is evident when a support structure, and the resultant shadow effect, is introduced into the analysis. Table 4 presents a summary of the percentage difference between the maximum and minimum total thrust and total torque values in a full blade rotation (for the analysis cases with support structures present). From this table, it can be seen that the difference in thrust force varies from 13% to 43%. Unsurprisingly, the effect is greater with the larger diameter support structures and when the structure is in front of the turbine rather than in its wake. These thrust force variances are similar to those observed by Frost et al. [12], who noted variances of 18% and 50% when there was a stanchion supporting the turbine located 1.8m downstream and upstream of the turbine, respectively, assuming a constant flow rate.

Please cite as: Finnegan, W.; Fagan, E.; Flanagan, T.; Doyle, A.; Goggins, J. (2020) Operational fatigue loading on tidal turbine blades using computational fluid dynamics. Renewable Energy, 152, p430-440DOI: 10.1016/j.renene.2019.12.154.

From Table 4, it can be seen that the difference in total torque varies much more significantly, i.e. from 29% to 73%. Once again, the effect is greater with larger diameter support structures and when the structure is in front of the turbine rather than in its wake. As the torque is directly proportional to the power that is generated by the turbine, it is vital that the location is optimised in order to reduce this effect and gain the maximum amount of power for an individual turbine.

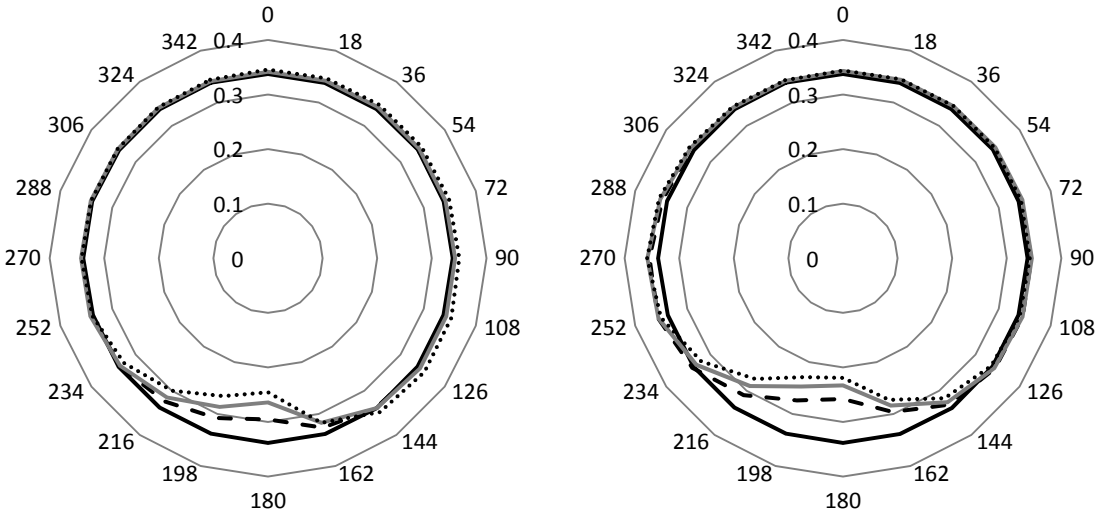

Figure 6: Variation of the thrust coefficient (C_T) of the blade, due to a constant flow of 2.25 m/s, as it moves through 360° from a vertical position (at 0°) when the support structure is: (a) in the wake of the turbine and (b) in front of the turbine

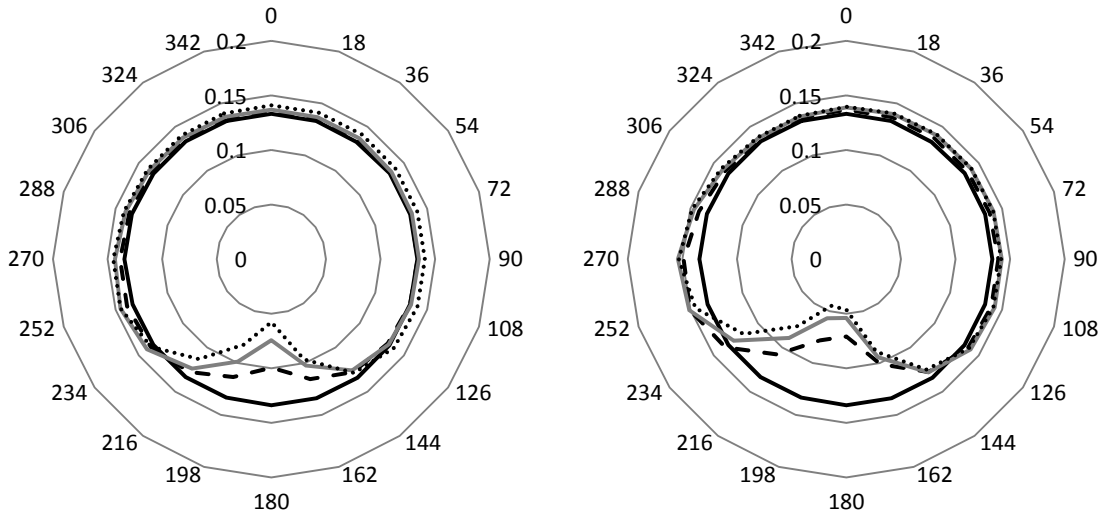

Please cite as: Finnegan, W.; Fagan, E.; Flanagan, T.; Doyle, A.; Goggins, J. (2020) Operational fatigue loading on tidal turbine blades using computational fluid dynamics. Renewable Energy, 152, p430-440DOI: 10.1016/j.renene.2019.12.154.

Figure 7: Variation of the power coefficient (C_P) of the blade, due to a constant flow of 2.25 m/s, as it moves through 360° from a vertical position (at 0°) when the support structure is: (a) in the wake of the turbine and (b) in front of the turbine

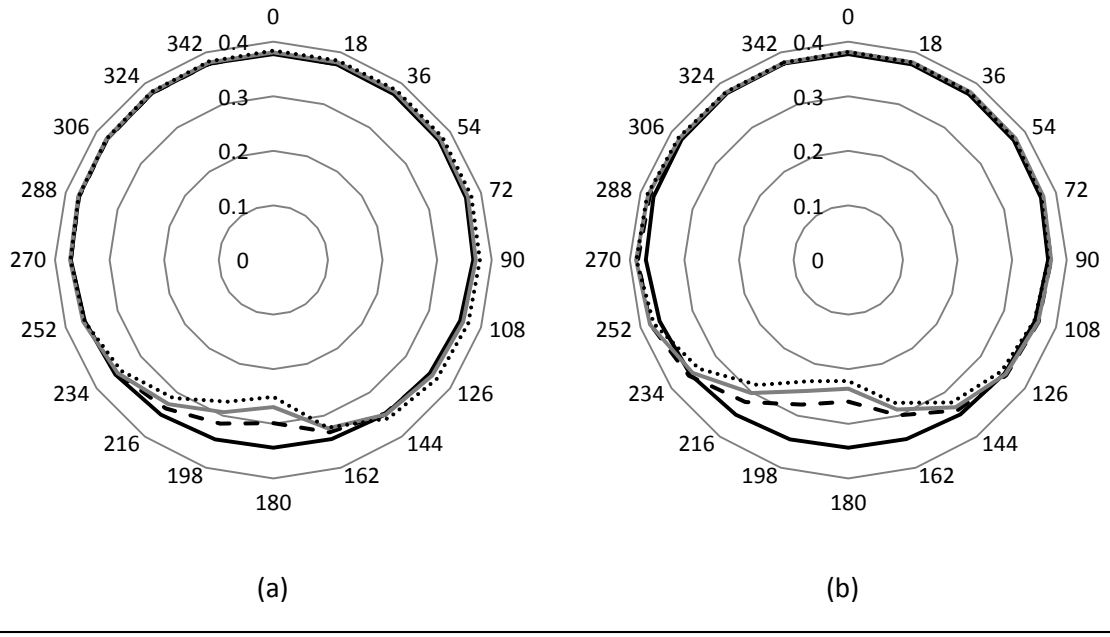

Figure 8: Variation of the thrust coefficient (C_T) of the blade, due to the mean tidal flow at Pentland Firth in Scotland (described in Section 2.3), as it moves through 360° from a vertical position (at 0°) when the support structure is: (a) in the wake of the turbine and (b) in front of the turbine

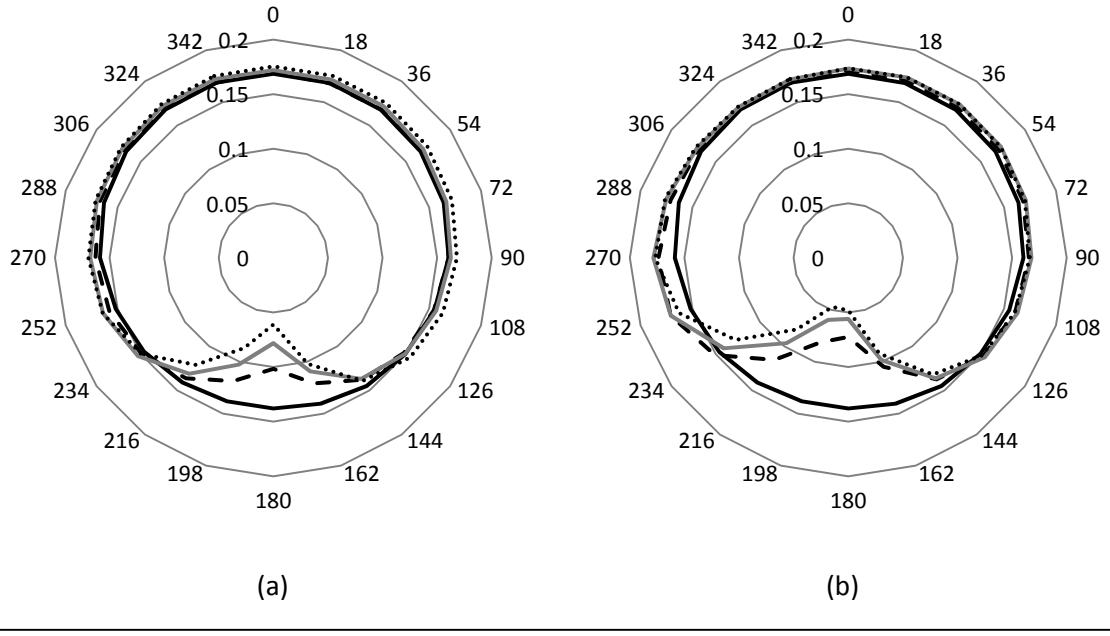

Figure 9: Variation of the power coefficient (C_P) of the blade, due to the mean tidal flow at Pentland Firth in Scotland (described in Section 2.3), as it moves through 360° from a vertical position (at 0°) when the support structure is: (a) in the wake of the turbine and (b) in front of the turbine

Please cite as: Finnegan, W.; Fagan, E.; Flanagan, T.; Doyle, A.; Goggins, J. (2020) Operational fatigue loading on tidal turbine blades using computational fluid dynamics. Renewable Energy, 152, p430-440DOI: 10.1016/j.renene.2019.12.154.

Table 4: A summary of the percentage difference between the maximum and minimum total thrust force and total torque as the blade rotates around 360° for each of the analysis cases with a support structure present, where d_{ss} is the diameter of the support structure

				Thrust force		Torque	
		d_{ss} (m)	d_{ss}/R	Constant flow	Mean flow	Constant flow	Mean flow
Location of support structure	In wake	1	0.12	13%	21%	29%	40%
		2	0.25	23%	29%	49%	55%
		3	0.37	31%	35%	60%	65%
	In Front	1	0.12	28%	33%	53%	58%
		2	0.25	35%	39%	65%	69%
		3	0.37	39%	43%	71%	73%

4 Conclusion

Although BEMT analysis is widely used and accepted as an industry standard when analysing the loadings on tidal turbine blades, CFD offers a good alternative, especially when the problem becomes increasingly complex. This is true for the scenario presented in this paper, where shadow effects due to the interaction between the tidal turbine and its support structure are being explored.

The magnitude of fatigue loading on tidal turbine blades is very significant (up to 43% of the maximum total thrust force on the blade, based on the analysis presented in this paper) and should be taken into account in all stages of design, testing and operational/maintenance phases of tidal turbine development. Therefore, the optimum tidal turbine and support structure design should be found that balances the structural capacity of the support structure with the resultant fatigue loading on the turbine blades. Additionally, if a support structure can be employed that minimises the impact of the flow on the turbine (especially in the in-front position) then it should be given high priority, since the resultant design will yield less maintenance to blades due to fatigue. The investigation of the effect of an unsteady loading on the turbine may also have significant impact on the blade fatigue design life and this will be explored in a follow up study, where the loading from surface waves is also included. Another avenue of investigation would be the unsteady loading on the blades due to turbulence von Kármán like vortices in the wake of the supporting structure, when it is in front of the turbine, which would require an unsteady Reynolds-averaged Navier-Stokes analysis.

Fatigue testing is well established in the wind energy sector, which is detailed in the structural testing standards DNV-DS-J102 [24] and IEC61400-23 [25]. For the tidal energy sector, a discussion of the requirements for fatigue testing blades and components is presented in the tidal turbine design standard, DNVGL-ST-0164 [26], and aspects have been included in the IEC design requirements for marine energy systems, IEC TS 62600-2:2016 [27]. The research presented in this study can help to better define the potential impacts of fatigue loading on tidal turbine components and potentially feed into the fatigue testing and design of components, as companies move into the final TRLs and begin full commercialisation.

The key to success for a new renewable energy source, such as tidal energy, is to ensure the levelised cost of energy is kept to a minimum and, preferably, lower than alternative energy sources to aid its commercial competitiveness and attractiveness to investors. Advanced and comprehensive fatigue

Please cite as: Finnegan, W.; Fagan, E.; Flanagan, T.; Doyle, A.; Goggins, J. (2020) Operational fatigue loading on tidal turbine blades using computational fluid dynamics. Renewable Energy, 152, p430-440DOI: 10.1016/j.renene.2019.12.154.

testing will de-risk the technology as it will ensure that tidal turbine blades can withstand fatigue effects over their functional lifespan. The large variations in thrust and torque loads, along with the impact of combined edgewise and flapwise loading, cause damage to the turbine blades and the bending moment applied to the blade root and blade-hub connections needs to be accurately predicted. These aspects need to be efficiently accounted for in the design and manufacture stages, which affords designers the opportunity to balance the capital expenditure (CAPEX) and operational expenditure (OPEX), which are predominantly maintenance costs, yielding a more efficient and cost effective tidal turbine design.

Acknowledgements

This research was funded in part by Science Foundation Ireland (SFI) through the Marine and Renewable Energy Ireland (MaREI) research centre (Grant no. 12/RC/2302), Science Foundation Ireland (SFI) under Grant Number 16/IFB/4512, the Sustainable Energy Authority of Ireland (SEAI) through the Ocean ERA-NET Ocean Energy Prototype Research and Development Programme 2018 as part of the SEABLADE project (Award no.: 18/OCN/102) and the European Commission under the FloTEC project (Floating Tidal Energy Conversion, Funded under: Horizon 2020, Low Carbon Energy (LCE), Grant Number: 691916). The last author would also like to acknowledge the support of Science Foundation Ireland through the Career Development Award programme (Grant No. 13/CDA/2200). The authors would like to express their gratitude to the Irish centre for high-end computing (ICHEC) for the computation processing power provided. The authors would like to acknowledge Dr Philippe Gleizon and the Environmental Research Institute at the Centre for Energy and the Environment of the University of the Highlands and Islands, UK for their kind contribution of the ADCP data for the Inner Sound, Pentland Firth.

Please cite as: Finnegan, W.; Fagan, E.; Flanagan, T.; Doyle, A.; Goggins, J. (2020) Operational fatigue loading on tidal turbine blades using computational fluid dynamics. Renewable Energy, 152, p430-440DOI: 10.1016/j.renene.2019.12.154.

References

[1] Ocean Energy Forum, Ocean Energy Strategic Roadmap 2016, building ocean energy for Europe, Ocean Energy Forum, Brussels, Belgium, 2016.
[2] Orbital Marine Power, Latest News, 2019. https://orbitalmarine.com/news. (Accessed 10th December 2019).
[3] D. Magagna, R. Monfardini, A. Uihlein, JRC Ocean Energy Status Report: 2016 Edition EUR 28407 EN, Publications Office of the European Union JRC104799, Luxembourg, 2016.
[4] T.D. Corsatea, D. Magagna, Overview of European innovation activities in marine energy technology, European Commission, Brussels, Belgium, 2013.
[5] A.H. Day, A. Babarit, A. Fontaine, Y.P. He, M. Kraskowski, M. Murai, I. Penesis, F. Salvatore, H.K. Shin, Hydrodynamic modelling of marine renewable energy devices: A state of the art review, Ocean Engineering 108 (2015) 46-69.
[6] I. Masters, J. Chapman, M. Willis, J. Orme, A robust blade element momentum theory model for tidal stream turbines including tip and hub loss corrections, Journal of Marine Engineering & Technology 10(1) (2011) 25-35.
[7] A.S. Bahaj, A.F. Molland, J.R. Chaplin, W.M.J. Batten, Power and thrust measurements of marine current turbines under various hydrodynamic flow conditions in a cavitation tunnel and a towing tank, Renewable Energy 32(3) (2007) 407-426.
[8] F. O'Rourke, F. Boyle, A. Reynolds, D.M. Kennedy, Hydrodynamic performance prediction of a tidal current turbine operating in non-uniform inflow conditions, Energy 93, Part 2 (2015) 2483-2496.
[9] P.W. Galloway, L.E. Myers, A.S. Bahaj, Quantifying wave and yaw effects on a scale tidal stream turbine, Renewable Energy 63 (2014) 297-307.
[10] E. Fagan, Design of fibre-reinforced polymer composite blades for wind and tidal turbines (PhD thesis), Civil Engineering, National University of Ireland Galway, Galway, Ireland, 2017.
[11] M. Badshah, S. Badshah, J. VanZwieten, S. Jan, M. Amir, S.A. Malik, Coupled Fluid-Structure Interaction Modelling of Loads Variation and Fatigue Life of a Full-Scale Tidal Turbine under the Effect of Velocity Profile, Energies 12(11) (2019) 2217.
[12] C. Frost, C.E. Morris, A. Mason-Jones, D.M. O'Doherty, T. O'Doherty, The effect of tidal flow directionality on tidal turbine performance characteristics, Renewable Energy 78 (2015) 609-620.
[13] U. Ahmed, D.D. Apsley, I. Afgan, T. Stallard, P.K. Stansby, Fluctuating loads on a tidal turbine due to velocity shear and turbulence: Comparison of CFD with field data, Renewable Energy 112 (2017) 235-246.
[14] P. Jeffcoate, R. Starzmann, B. Elsaesser, S. Scholl, S. Bischoff, Field measurements of a full scale tidal turbine, International Journal of Marine Energy 12 (2015) 3-20.
[15] M. Lewis, S.P. Neill, P. Robins, M.R. Hashemi, S. Ward, Characteristics of the velocity profile at tidal-stream energy sites, Renewable Energy 114 (2017) 258-272.
[16] G.S. Bir, M.J. Lawson, Y. Li, Structural Design of a Horizontal-Axis Tidal Current Turbine Composite Blade, (44373) (2011) 797-808.
[17] C.R. Kennedy, V. Jaksic, S.B. Leen, C.M.Ó. Brádaigh, Fatigue life of pitch- and stall-regulated composite tidal turbine blades, Renewable Energy 121 (2018) 688-699.
[18] E.M. Fagan, C.R. Kennedy, S.B. Leen, J. Goggins, Damage mechanics based design methodology for tidal current turbine composite blades, Renewable Energy 97 (2016) 358-372.
[19] C. Faudot, O.G. Dahlhaug, Prediction of Wave Loads on Tidal Turbine Blades, Energy Procedia 20 (2012) 116-133.
[20] I.A. Milne, A.H. Day, R.N. Sharma, R.G.J. Flay, The characterisation of the hydrodynamic loads on tidal turbines due to turbulence, Renewable and Sustainable Energy Reviews 56 (2016) 851-864.
[21] ANSYS, ANSYS® CFX (Release 17.1): CFX-Solver Theory Guide, , ANSYS Inc., 2017.
[22] W. Finnegan, E. Fagan, S. Leen, J. Goggins, CFD Simulation and FEM Structural Analysis of Tidal Turbine Blades, 12th European Wave and Tidal Energy Conference (EWTEC2017), Cork, Ireland, 2017.
[23] Gardline Surveys, Pentland Firth Tidal Stream Observations. Tech. Rep. 5699, 2001.

Please cite as: Finnegan, W.; Fagan, E.; Flanagan, T.; Doyle, A.; Goggins, J. (2020) Operational fatigue loading on tidal turbine blades using computational fluid dynamics. Renewable Energy, 152, p430-440DOI: 10.1016/j.renene.2019.12.154.

[24] DNV GL, Design and manufacture of wind turbine blades, offshore and onshore wind turbines, DNV Standard, DNV-DS-J102, 2010, pp. 2010-11.
[25] International Electrotechnical Commission (IEC), Part 23: Full-scale structural testing of rotor blades, IEC 61400-23:2014 Wind turbines 2014.
[26] DNV GL, Tidal turbines, DNV Standard, DNVGL-ST-0164, Oslo, Norway, 2015.
[27] I.E.C. (IEC), IEC TS 62600-2:2016 Marine energy - Wave, tidal and other water current converters - Part 2: Design requirements for marine energy systems, International Electrotechnical Commission (IEC), Geneva, Switzerland, 2016.
[28] M. Badshah, S. Badshah, K. Kadir, Fluid Structure Interaction Modelling of Tidal Turbine Performance and Structural Loads in a Velocity Shear Environment, Energies 11(7) (2018) 1837.
[29] D.L. Aparna, R.T. Naayagi, M. Ramadan, CFD analysis of tidal turbine blades, TENCON 2017 - 2017 IEEE Region 10 Conference, 2017, pp. 2708-2711.
[30] S. Tatum, M. Allmark, C. Frost, D. O'Doherty, A. Mason-Jones, T. O'Doherty, CFD modelling of a tidal stream turbine subjected to profiled flow and surface gravity waves, International Journal of Marine Energy 15 (2016) 156-174.
[31] M.G. Gebreslassie, S.O. Sanchez, G.R. Tabor, M.R. Belmont, T. Bruce, G.S. Payne, I. Moon, Experimental and CFD analysis of the wake characteristics of tidal turbines, International Journal of Marine Energy 16 (2016) 209-219.
[32] S.S. Kulkarni, C. Chapman, H. Shah, Computational Fluid Dynamics (CFD) Mesh Independency Study of A Straight Blade Horizontal Axis Tidal Turbine, (2016).
[33] M.A. Holst, O.G. Dahlhaug, C. Faudot, CFD Analysis of Wave-Induced Loads on Tidal Turbine Blades, IEEE Journal of Oceanic Engineering 40(3) (2015) 506-521.
[34] R. Noruzi, M. Vahidzadeh, A. Riasi, Design, analysis and predicting hydrokinetic performance of a horizontal marine current axial turbine by consideration of turbine installation depth, Ocean Engineering 108 (2015) 789-798.
[35] X. Wang, A.H. Day, CFD Turbulence Modelling of Tidal Turbine Unsteady Blade Load, 11th European Wave and Tidal Energy Conference, Nantes, France, 2015.
[36] C.-H. Jo, D.-Y. Kim, Y.-H. Rho, K.-H. Lee, C. Johnstone, FSI analysis of deformation along offshore pile structure for tidal current power, Renewable Energy 54 (2013) 248-252.
[37] S. Kang, I. Borazjani, J.A. Colby, F. Sotiropoulos, Numerical simulation of 3D flow past a real-life marine hydrokinetic turbine, Advances in Water Resources 39 (2012) 33-43.
[38] S.R. Turnock, A.B. Phillips, J. Banks, R. Nicholls-Lee, Modelling tidal current turbine wakes using a coupled RANS-BEMT approach as a tool for analysing power capture of arrays of turbines, Ocean Engineering 38(11–12) (2011) 1300-1307.
[39] C. Faudot, O.G. Dahlhaug, Tidal turbine blades: Design and dynamic loads estimation using CFD and blade element momentum theory, 30th International Conference on Ocean, offshore and Artic Engineering, Rotterdam, The Netherlands, 2011.
[40] T. O'Doherty, A. Mason-Jones, D.M. O'Doherty, C.B. Byrne, I. Owen, Y.X. Wang, Experimental and Computational Analysis of a Model Horizontal Axis Tidal Turbine, 8th European Wave and Tidal Energy Conference, Uppsala, Sweden, 2009.